AN GROUND AND UNDER-GROUND URBAN ROADS SURVEYING APPROACH USING INTEGRATED 3D LIDAR AND 3D GPR TECHNOLOGY

Yibo Zhou[1], Qingwu Hu[1]*, Ju Zhang[1], Pengcheng Zhao[1], Fei Yu[2], Mingyao Ai[1]

[1]School of Remote Sensing and Information Engineering, Wuhan University, China,
(zhouyibo, huqw, zhangju, pengcheng.zhao, aimingyao) @whu.edu.cn
[2]CCCC Second Highway Consultants Co., Ltd., China,
yufish1987@foxmail.com

KEY WORDS: LiDAR, Ground Penetrating Radar, Point-cloud, GPR C-Scan, Road Surveying, Smart City.

ABSTRACT:
Digitalization of urban roads is an important part of smart city construction. In addition to having a basic understanding of the structure of the transportation network, we need to have a preliminary understanding of the information around the road, the current status of the road, and the impact that municipal projects may have on the road. At present, the three-dimensional information of the ground parts of roads can be obtained efficiently and accurately on a large scale by using three-dimensional scanning technology. However, there is a lack of comprehensive and intuitive understanding of the under-ground information and a lack of synergistic consideration of the ground and under-ground information. In this paper, a ground and under-ground urban road surveying system based on 3D LiDAR and 3D ground penetrating radar (GPR) is presented. The system covers multi-sensor coordinated control, time-space datum setup, and post-processing data. Experiments show that the system can realize the integrated ground and under-ground 3D surveying for urban roads, generate intuitive three-dimensional point cloud map model of ground and under-ground of urban roads, and provide effective technical support for smart city construction.

1. INTRODUCTION

During the rapid development of cities, road conditions deserve attention. In order to facilitate the process of digital cities, provide digital documents for municipal projects, and provide known urban road status information for autonomous driving technologies, a basic understanding of the current condition of urban roads is required. Information on urban road conditions is both information that can be retained for a long time with few changes, including the city's existing urban road plan, road surrounding features and underground pipelines, and information that will change over time, with particular attention to possible ground changes and under-ground cavity diseases caused by road use and urban development. In order to understand the current status information of urban roads, we need to obtain the spatial distribution on the ground of urban roads on one hand, and also have a preliminary understanding of the situation under-ground on the other hand. In order to achieve this goal, we propose a strategy of three-dimensional surveying of urban roads integrated ground and under-ground.

Many studies have been conducted in the past for spatial 3D surveying and reconstruction. Ground can be surveying by various techniques such as LiDAR, photogrammetry, and computer vision. These include using LiDAR for surveying and extraction of houses and roads (Rottensteiner et al., 2005), building height prediction (Park and Guldmann, 2019), completing automated 3D city reconstruction (Garcíamoreno et al., 2012), using tilted aerial imagery to give texture information to 3D city models (Frueh et al., 2004), using UAV tilt photography to complete 3D city modeling (Wang et al., 2015), using Google Earth imagery and ground images for 3D city modeling (Ding et al., 2007), and using Google Street View for 3D city modeling (Torii et al., 2009). Underground can be surveyed non-destructively by ground-penetrating radar, ultrasonic, thermal infrared, and nuclear magnetic resonance techniques. These include detecting leaks in water pipelines using ground-penetrating radar (Bimpas et al., 2010), completing 3D reconstruction of underground defects using ultrasound (Zheng and Yao, 2021), determining the area and depth of underground defects using thermal infrared (Ma and Ma, 2011), and detecting groundwater hazards in tunnels and mines using nuclear magnetic resonance techniques (Lin et al., 2020).

* Corresponding author

Current ground and under-ground studies are mainly conducted separately, thus resulting in incoherent between ground and under-ground data, which is not conducive to more comprehensive and intuitive research and applications. Some studies have started to experiment with the combined analysis of LiDAR and GPR, for example, Aqeel used LiDAR with GPR measure the orientations of hidden subvertical joints in highways rock cuts (Aqeel, 2012), Webb combined GPR with LiDAR to estimate the spatial distribution of liquid water content in seasonal snowpacks (Webb et al., 2018).

In this paper, an integrated ground and under-ground 3D surveying system is proposed for ground and under-ground data fusion analysis, including hardware composition, equipment coordination, and subsequent processing of data. The system mainly consists of a LiDAR surveying system and a GPR surveying system, and the related hardware is mounted on a cart. We survey the main roads or minor roads in the study area and generate a 3D point cloud map model of the roads after data processing, thus completing the digitization of ground and under-ground urban roads.

2. SYSTEM COMPOSITION AND WORKING PRINCIPLE

The composition of the integrated ground and under-ground 3D surveying system is shown in **Figure 1.**

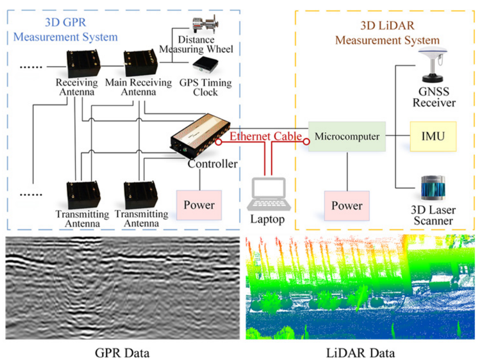

Figure 1. Composition of the integrated ground and under-ground 3D surveying system

The hardware of the 3D GPR surveying system includes receiving antennas, transmitting antennas, distance measuring wheel, GPS timing clock, controller, and power supply. The 3D GPR includes six receiving antennas and seven transmitting antennas, with the antenna center frequency of 450MHz, using three-dimensional array configuration, each receiving antenna is connected to two transmitting antennas through coaxial cable, and each receiving antenna is also connected to the adjacent receiving antenna, forming 12 channels. The detection width of the 3D GPR surveying system was 0.9 m. It has a resolution of approximately 0.04 m in general soil, at a depth of 5 m. The electromagnetic wave signal is sent to the ground through the transmitting antenna and is reflected when it meets the ground with a large difference in dielectric coefficient, and the reflected signal is received by the neighboring receiving antenna. The GPR controller coordinates the signals sent and received by the antennas, and to perform preliminary signal processing, converting the electromagnetic wave signals into digital signals. The GPS timing clock is used to time the 3D GPR surveying process, so that the data obtained includes UTC time.

The hardware of 3D LiDAR surveying system contains 3D laser scanner, inertial measurement unit (IMU), GNSS receiver, microcomputer control unit, and power supply. The 3D LiDAR scanner adopts a hybrid solid-state LiDAR approach, which collects 32 laser transceiver components. The vertical field of view of the system is 31 degrees with a vertical angle resolution of 1 degree, the horizontal field of view is 360 degrees with a horizontal angle resolution of 0.18 degrees 32 laser transmitter components rotate rapidly while emitting high-frequency laser beams for continuous scanning of the external environment. The inertial measurement unit is used to measure the instantaneous acceleration and instantaneous angular velocity of the system in xyz three directions during the propulsion process in real time, and the initial position and reference direction are used to complete the shortcut solution independently to provide the basis for subsequent solution positioning. After differential positioning, the position of the equipment can be accurately positioned. The microcomputer control unit coordinates the sensors in the 3D LiDAR to ensure the uniformity of time and space reference for data acquisition.

3. KEY TECHNOLOGIES

In order to complete the integrated ground and under-ground three-dimensional surveying, there exists the key problems of coordinating the simultaneous measurement of ground and under-ground equipment and the stitching of ground and under-ground data. In this chapter, three key technologies are proposed, including the unification of time-space measurement datum of 3D GPR surveying system and 3D LiDAR surveying system, 3D GPR data processing, and 3D GPR coordinate processing.

3.1 Unification of time and space references

In order to integrate the ground and under-ground surveying system and ensure the consistency and reliability of the modeling results of both parties, we set a consistent reference datum for 3D GPR data and 3D LiDAR data. We use UTC time as the time reference for the system to achieve time synchronization control, and WGS84 coordinates as the spatial reference for the system to achieve unified spatial coordinate system. The data connection is shown in **Figure 2**:

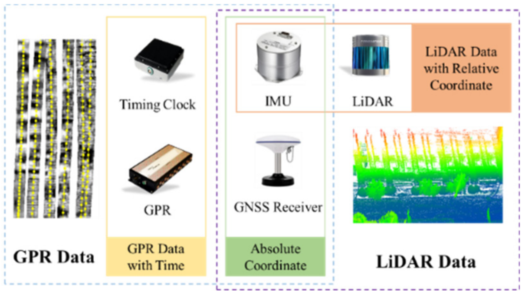

Figure 2. System data collaboration

The original GPR data only contains time but does not contain position coordinates, and the original LiDAR data only contains relative position. In the survey process using the same set of GNSS receiving system, after decoding we can get the accurate coordinates of the equipment operation process. We use the precise coordinates to match the 3D GPR and 3D LiDAR data according to the standard time, so that we can get the ground and under-ground data with unified time and space reference, which is convenient for data stitching in the later stage.

3.2 3D GPR data processing

Due to the complexity of the subsurface medium, the signal-to-noise ratio of the raw under-ground data is much lower than that of the ground data. The raw data contain various noises that make the effective information may be masked, so some methods are needed to suppress the noise, enhance the signal and improve the data signal-to-noise ratio. We can extract characteristic information such as velocity, amplitude, frequency, phase, etc. from the processed data to help the interpreter to geologically interpret the data. 3D GPR data processing can be divided into three main parts, data editing, noise suppression, and data enhancement(Jol, 2008).

Data editing is mainly aimed at the DC drift contained within the data, we need to suppress the DC component, as described in **Equation (1)**. Noise suppression is mainly aimed at the interference signals with more obvious demarcation from the effective signal spectrum distribution, which can be processed by the band-pass filtering, as shown in **Equation (2)**. The data enhancement is mainly for the gradual decay of the reflected wave amplitude in the time axis due to the wavefront diffusion and the absorption of the electromagnetic wave by the medium. The return wave amplitude A_0 can be calculated as **Equation (3)**.

$$X'(n,t) = X(n,t) - \frac{1}{N}\sum_{k=1}^{N} X(n,k) \tag{1}$$

Where $X(n,k)$ = the intensity value of the data

$$H(f) = \begin{cases} 0 & f < f_1 \\ \sin^2 \frac{\pi}{2}\left(\frac{f-f_1}{f_2-f_1}\right) & f_1 \leqslant f \leqslant f_2 \\ 1 & f_2 < f < f_3 \\ \sin^2 \frac{\pi}{2}\left(\frac{f_4-f}{f_4-f_3}\right) & f_3 \leqslant f \leqslant f_4 \\ 0 & f > f_4 \end{cases} \tag{2}$$

Where f_1, f_2, f_3, f_4 = the cut-off frequency values derived from a priori knowledge
$H(f)$ = the weight of the signal strength

$$A_0 = Avte^{\alpha t} \tag{3}$$

Where A_0 = return wave amplitude

A = the electromagnetic wave amplitude
α = the absorption coefficient
t = two-way time of the reflected return wave
v = propagation speed of the electromagnetic wave in the medium

With the above processing, 3D GPR images can be generated based on the signal intensity, and the relevant interpretation of underground conditions can be performed based on the apparent differences between the features therein and the background.

3.3 3D GPR data positioning

The position information of the GNSS antenna is obtained directly by the system, and a series of conversions are required to obtain the true coordinates of the 3D GPR data in (Xu and He, 2019). The position state of equipment while surveying is shown in **Figure 3**.

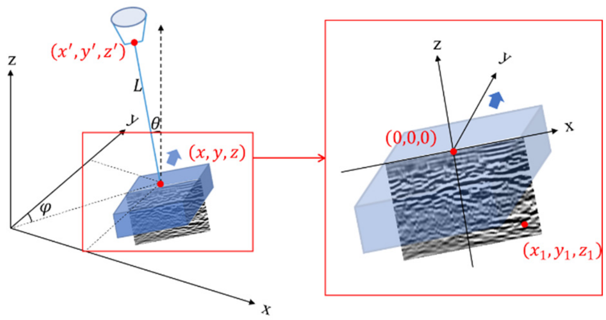

Figure 3. The position state of 3D GPR equipment

Firstly, the GNSS coordinates need to be tilt corrected to calculate the corresponding WGS84 coordinates for the sampled point data. The **Equation (4)** of tilt correction is shown as follows, pitch and yaw can be derived from the inertial guidance measurement unit.

$$\begin{cases} x = x' + \Delta x = x' + L\sin\theta\cos\varphi \\ y = y' + \Delta y = y' + L\sin\theta\sin\varphi \\ z = z' + \Delta z = z' + L\cos\theta \end{cases} \tag{4}$$

Where θ = pitch
φ = yaw
L = distance of GNSS receiver from the ground-penetrating radar antenna
(x', y', z') = coordinates received by GNSS antenna
(x, y, z) = coordinates of the sampling point of the equipment

The coordinates of the sampling points of the multi-channel 3D GPR correspond to the data coordinate centers, and the data collected at a single location are shown in the **Figure 3**. The world coordinates of the data point can be derived from the **Equation (5)**, yaw, pitch, and roll are derived from the IMU.

$$\begin{bmatrix} X \\ Y \\ Z \end{bmatrix} = \begin{bmatrix} x \\ y \\ z \end{bmatrix} + \begin{bmatrix} a_1 & a_2 & a_3 \\ b_1 & b_2 & b_3 \\ c_1 & c_2 & c_3 \end{bmatrix} \begin{bmatrix} x_1 \\ y_1 \\ z_1 \end{bmatrix} \tag{5}$$

$$\begin{cases} a_1 = \cos\theta\cos\varphi \\ a_2 = -\cos\psi\sin\varphi + \sin\psi\sin\theta\cos\varphi \\ a_3 = \sin\psi\cos\varphi + \cos\psi\sin\theta\cos\varphi \\ b_1 = \cos\theta\sin\varphi \\ b_1 = \cos\theta\sin\varphi \\ b_2 = \cos\psi\cos\varphi + \sin\psi\sin\theta\sin\varphi \\ b_3 = -\sin\psi\cos\varphi + \cos\psi\sin\theta\sin\varphi \\ c_1 = -\sin\theta \\ c_2 = \sin\psi\cos\theta \\ c_3 = \cos\psi\cos\varphi \end{cases}$$

Where θ = pitch
φ = yaw
ψ = roll
(x_1, y_1, z_1) = relative coordinates inside the data
(X, Y, Z) = world coordinates of the data point
(x, y, z) = world coordinates of the sampling point of the equipment

Based on the world coordinates and the signal strength value of the 3D GPR data, the 3D GPR image can be converted into 3D point cloud format. At this time, the 3D GPR data adopts the same world coordinate system as the 3D LiDAR point cloud data, and both are in point cloud format, which can complete the fusion of the two point clouds and generate an integrated ground and under-ground3D point cloud map model.

4. EXPERIMENT AND DISCUSSION

4.1 Experimental equipment and site

The integrated ground and under-ground surveying equipment is shown in Figure 4, the upper part of the main body is a 3D LiDAR surveying system, and the lower part of the main body is a 3D GPR surveying system.

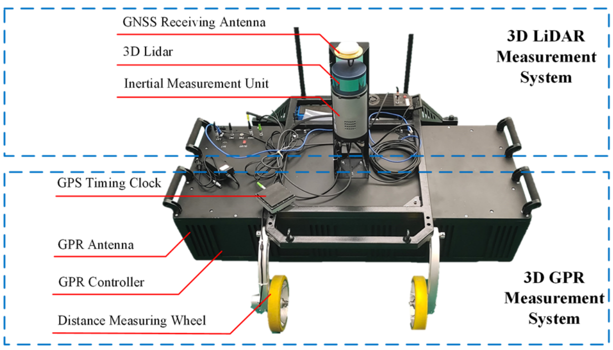

Figure 4. the integrated ground and under-ground 3D surveying equipment

The experimental site was chosen as the road around Wuhan University Zall Stadium, and **Figure 5** shows the satellite image of Wuhan University Zall Stadium, with the red line representing the surveying path.

Figure 5. satellite image of Wuhan University Zall Stadium

The road around Zall Stadium is about 872 meters long and 6 meters wide. The area around the stadium is open and unobstructed, and high quality of GNSS signal can be obtained, which can provide more accurate positioning data for the system. There are a certain amount of trees and buildings around, which can provide data support for the verification of the 3D LiDAR surveying system, and there are pipes and some unevenly distributed media areas below the road, which can provide data support for the verification of the 3D GPR surveying system.

4.2 Data acquisition and Processing

The process of data acquisition using integrated ground and under-ground surveying equipment is shown in **Figure 6.**

Figure 6. Data acquisition using integrated ground and under-ground surveying equipment

The general steps of data acquisition are as follows:

First, system time synchronization and attitude calibration. Before the measurement starts, turn on the power system of the equipment in a place with good GNSS signal quality, check the GNSS receiver and GPS timing clock satellite signal reception to ensure good GNSS signal quality. At this time, the system automatically unifies the timing of the 3D LiDAR scanner, inertial measurement unit and 3D ground-penetrating radar antenna. Then open the 3D LiDAR scanning system control software in the control computer, and keep the whole system stationary for a period of time after creating a new project. The system will calibrate the GNSS receiver and IMU in the stationary process for the positional attitude, obtain the corrected stable coordinates, correct the automatic change of the gyroscope of the inertial unit, and calculate the zero offset error of the IMU.

Second, data acquisition. Set the parameters of each part of the measurement on the control computer, push the system trolley along the planned route in the detection area, and start the integrated ground and under-ground surveying. GPS timing clock and GNSS receiver obtain time and positioning information, IMU obtains velocity and angle information, 3D LiDAR system collects ground ground point cloud data, and 3D GPR system collects under-ground media distribution data. As the single surveying width of 3D GPR is limited, the linear measurement may not completely cover the whole detection area, and several round-trip measurements are needed to ensure that the whole measurement area is swept.

Third, static convergence and then end the survey. After the LiDAR data and GPR data acquisition is completed, save the data and turn off the 3D LiDAR system and 3D GPR system. Push the equipment to the area with good GNSS signal to settle and converge, and turn off all sensors after convergence to finish the data acquisition work.

After the acquisition work is completed, data processing is carried out. Firstly, based on the GNSS/INS tightly coupled position solution, get accurate position information of the acquisition process, so as to assign coordinate information to the obtained 3D ground-penetrating radar data; secondly, respectively, 3D LiDAR data and 3D ground-penetrating radar data for the corresponding processing and interpretation work; finally, the 3D GPR image is converted into point cloud data, which will be combined with the processed 3D LiDAR data, and then a three-dimensional detection point cloud map of the ground and under-ground can be obtained.

4.3 RESULT

Figure 7 shows some of the 3D GPR images after data processing and interpretation. Figure 7(a)(b) shows the 3D GPR images containing pipes, and Figure 7(c)(d) shows the 3D GPR images containing shafts. By analyzing the processed 3D ground-penetrating radar images, it is obvious to determine the type, location, contour and other information of the possible underground features.

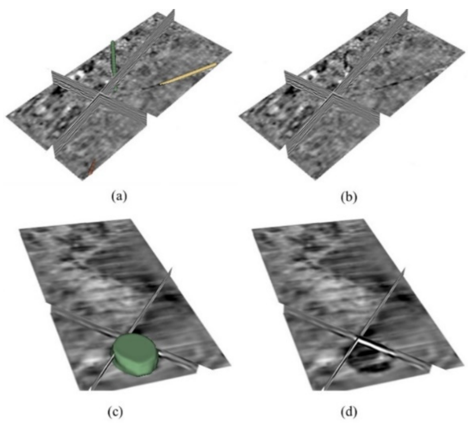

Figure 7. 3D GPR images

Figure 8 shows part of the 3D LiDAR point cloud map after data processing. Figure 8(a) shows the imaging effect of road signs on the 3D point cloud, Figure 8(b) shows the imaging effect of street trees on the 3D point cloud, and Figure 8(c) shows the imaging effect of buildings around the road on the 3D point cloud. The 3D point cloud can accurately reconstruct the location and outline of the main features around the road, and analyzing the 3D point cloud map can provide detailed and accurate information about the road condition.

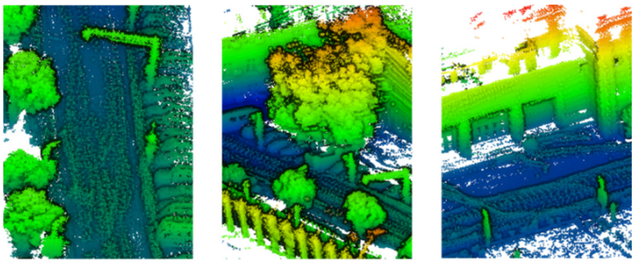

(a) (b) (c)

Figure 8. 3D point cloud map

Figure 9 shows the full range of ground-penetrating radar images of the roads around the Zall Stadium. Due to the large amount of data, it is necessary to process the data in chunks. We cut the data into 26 chunks as marked in the figure, and then re-spliced them after processing.

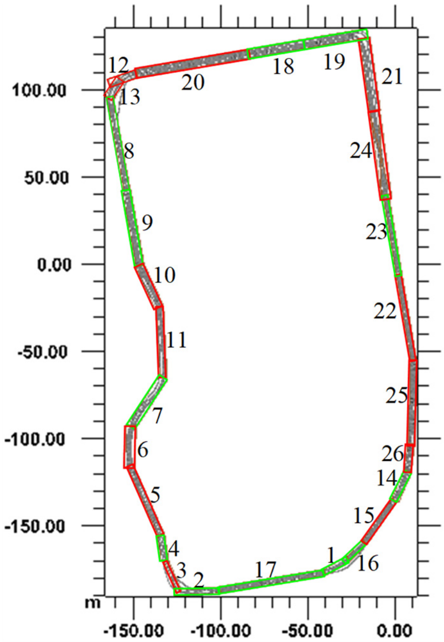

Figure 9.3D GPR image of the road around the Zall Stadium

Figure 10 shows the 3D point cloud map obtained from the 3D LiDAR data. It has a high positioning match with the GPR data and a small stitching error, and can complete the subsequent ground and under-ground data fusion stitching work.

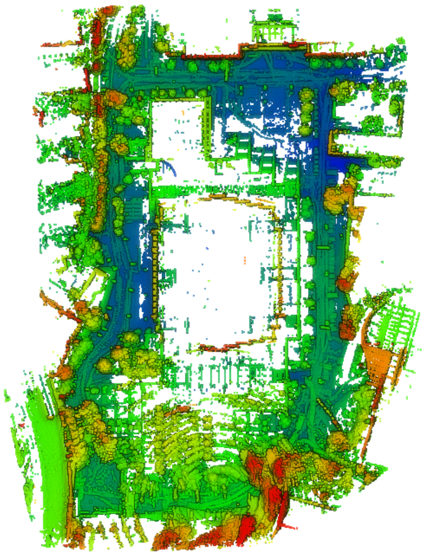

Figure 10. 3D point cloud map of the road around the Zall Stadium

Figure 11 shows the 3D point cloud map after the fusion of ground and under-ground data. The ground and under-ground data are well spliced and fused without gaps and voids, and the quality of the obtained data is high, which proves that the technical solution proposed in this paper is effective. By analyzing the ground and under-ground information, the road condition can be understood accurately, clearly and quickly. If there is a problem, it can be quickly located and quickly come up with a solution according to the site situation in time.

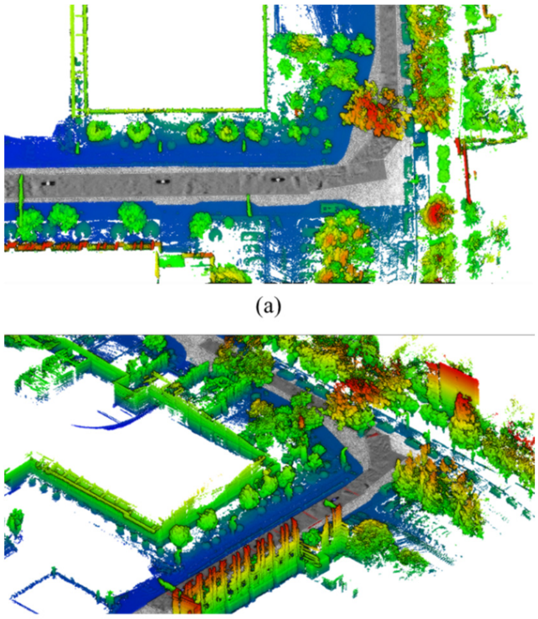

(a)

(b)

Figure 11. Part of the 3D point cloud map after fusion

Figure 12 shows the profile of the ground and under-ground 3D point cloud maps. If there is a situation such as a cavity in the road, the profile can be used to quickly and accurately determine the state of the road above the cavity and whether there are other features that may further cause the road to collapse. Through the fusion analysis of ground and under-ground data, a more comprehensive and intuitive judgment of road problems can be made.

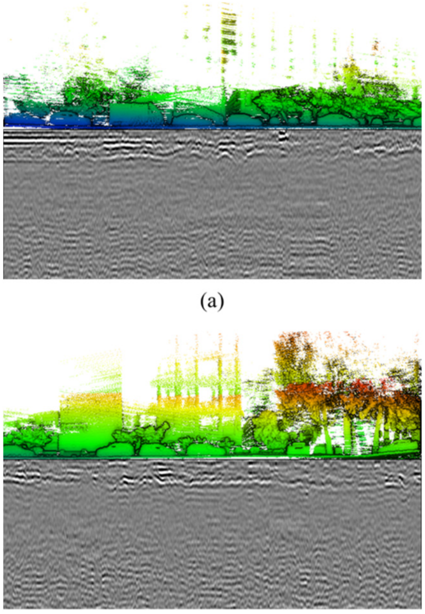

(a)

(b)

Figure 12. 3D point cloud map profile

In the 3D point cloud map, some under-ground information may be obscured. We decode the effective information in it, and highlight the three-dimensional contours of pipelines, shafts and other features, the display effect is shown in **Figure 13**. The ground and under-ground three-dimensional point cloud map has been basically formed, which can provide clear and effective a priori information for road maintenance and municipal engineering.

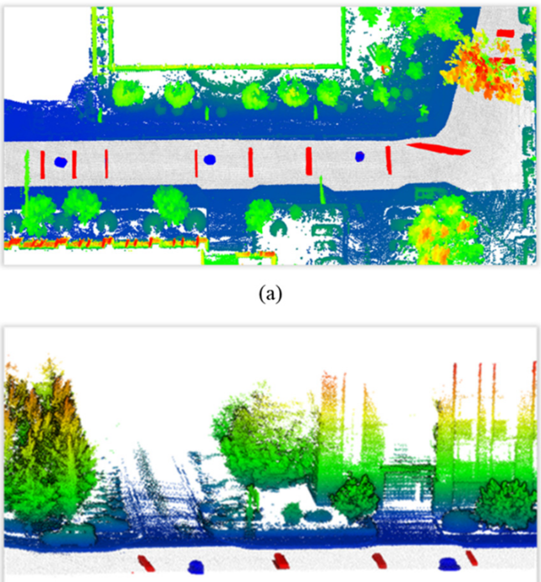

(a)

(b)

Figure 13. 3D point cloud map with subsurface target interpretation

5. CONCLUSION

This paper introduces an integrated ground and under-ground 3D surveying system combining 3D LiDAR technology and 3D GPR technology, and introduces the system composition, working principle, and key technologies to realize the integrated ground and under-ground data collaboration. It can effectively complete the ground and under-ground integrated urban road 3D detection, realize the ground and under-ground 3D data stitching, generate ground and under-ground integrated 3D point cloud map, provide effective digital information for the construction of digital city, and provide timely and intuitive 3D information for municipal road maintenance work. In the future, the use of integrated ground and under-ground 3D surveying system can play a key role in road quality inspection, digital city construction. The ground and under-ground integrated urban road three-dimensional detection system, with a wide range of application, strong portability, high measurement efficiency, post-processing simple and fast, but there are still the following two points can be improved: First, the system contains the relevant technology, does not include mature automatic feature recognition, so it needs to have the knowledge of LiDAR and ground-penetrating radar personnel to interpret; Second, limited by hardware factors, three-dimensional GPR 's surveying width is limited, currently need to let the scanning range cover the measurement area, but the 3D LiDAR measurement range is wide, in the same road may produce too much redundant data.

REFERENCE

Aqeel, A.M., 2012. Measuring the orientations of hidden subvertical joints in highways rock cuts using ground penetrating radar in combination with LIDAR. Missouri University of Science and Technology.

Bimpas, M., Amditis, A., Uzunoglu, N., 2010. Design and implementation of an integrated high resolution imaging ground penetrating radar for water pipeline rehabilitation, in: Radar Symposium.

Ding, W., Zhu, F., Hao, Y., 2007. Interactive 3D city modeling using Google Earth and ground images, in: Fourth International Conference on Image and Graphics (ICIG 2007). IEEE, pp. 849–854.

Frueh, C., Sammon, R., Zakhor, A., 2004. Automated texture mapping of 3D city models with oblique aerial imagery, in: International Symposium on 3d Data Processing.

Garcíamoreno, A.I., Gonzalezbarbosa, J., Hurtadoramos, J.B., Ramirezpedraza, A., Gonzálezbarbosa, E.A., 2012. Automatic 3D city reconstruction platform using a LIDAR and DGPS., in: Springer Berlin Heidelberg.

Jol, H.M., 2008. Ground penetrating radar theory and applications. elsevier.

Lin, J., Zhu, J., Wang, H., Teng, F., Zhang, Y., 2020. A review on the progress of the underground nuclear magnetic resonance method for groundwater disaster forecasting detection of tunnels and mines. Journal of Applied Geophysics 177, 104041.

Ma, S., Ma, Q., 2011. Modified Infrared Images Contrast for Pulsed Thermography, in: Measuring Technology and Mechatronics Automation (ICMTMA), 2011 Third International Conference On.

Park, Y., Guldmann, J.M., 2019. Creating 3D city models with building footprints and LIDAR point cloud classification: A machine learning approach. Computers, Environment and Urban Systems 75, 76–89.

Rottensteiner, F., Trinder, J., Clode, S., 2005. Data acquisition for 3D city models from LIDAR extracting buildings and roads, in: IEEE International Geoscience & Remote Sensing Symposium.

Torii, A., Havlena, M., Pajdla, T., 2009. From Google Street View to 3D City models, in: IEEE International

Conference on Computer Vision Workshops.

Wang, L., Zheng-Peng, W.U., Jiang, X.Y., Chen, C., 2015. Application of the UAV Oblique Photography Technique in 3D City Modeling. Geomatics & Spatial Information Technology.

Webb, R.W., Jennings, K.S., Fend, M., Molotch, N.P., 2018. Combining ground-penetrating radar with terrestrial LiDAR scanning to estimate the spatial distribution of liquid water content in seasonal snowpacks. Water Resources Research 54, 10,339-10,349.

Xu, C., He, J., 2019. Research on Tilt Survey Algorithm Based on Accelerometer and GNSS Receiver Data Fusion, in: Advanced Multimedia and Ubiquitous Engineering. Springer, pp. 71–77.

Zheng, K., Yao, Y., 2021. Automatic three-dimensional reconstruction of subsurface defects by segmenting ultrasonic point cloud. Journal of the Taiwan Institute of Chemical Engineers 120.